Electronic Supplementary Material (ESI) for Dalton Transactions.

$RbSe_3B_2O_9(OH)$ and $CsSe_3B_2O_9(OH)$: One Dimensional Boroselenite-based Anionic frameworks with Second Harmonic Gerneration Properties

Jian-Han Zhang,* Qi-Bing Wang, Chun-Le Chen, Ju-Xiang Luo, Chun-Li Hu, Jun-Ling Song, and Jiang-Gao Mao*

Supporting Information

Table of contents

Experimental section

1. Synthesis of compounds
2. Structure determination
3. Physical Properties Measurements
4. Computational Descriptions
5. Reference

Table S1. Important bond lengths (Å) for the $RbSe_3B_2O_9(OH)$ and $CsSe_3B_2O_9(OH)^a$

Table S2. Assignments of IR absorption peaks for $RbSe_3B_2O_9(OH)$ and $CsSe_3B_2O_9(OH)$.

Table S3. The state energies (eV) of the lowest conduction band (LCB) and the highest valence band (HVB) of $RbSe_3B_2O_9(OH)$, and $CsSe_3B_2O_9(OH)$.

Figure S1. SEM images with different magnification for $RbSe_3B_2O_9(OH)$ (a) and $CsSe_3B_2O_9(OH)$ (b).

Figure S2. Simulated and measured XRD powder patterns for $RbSe_3B_2O_9(OH)$ (a) and $CsSe_3B_2O_9(OH)$ (b).

Figure S3. IR spectra for $RbSe_3B_2O_9(OH)$ (a) and $CsSe_3B_2O_9(OH)$ (b).

Figure S4. Diffuse reflectance UV-vis-NIR spectra for $RbSe_3B_2O_9(OH)$ (a) and $CsSe_3B_2O_9(OH)$ (b) are scaled to emphasize direct and indirect optical transitions. The degree of linear overlapping suggests the type of optical transition.

Figure S5. The imaginary parts of the frequency-dependent dielectric function of $RbSe_3B_2O_9(OH)$ (a) and $CsSe_3B_2O_9(OH)$ (b).

Figure S6. The curves of the averaged imaginary part and real part of dielectric function of

$RbSe_3B_2O_9(OH)$ (a) and $CsSe_3B_2O_9(OH)$ (b).

Figure S7. The dispersion of refractive index of $RbSe_3B_2O_9(OH)$ (a) and $CsSe_3B_2O_9(OH)$ (b).

1. Synthesis of compounds

All of the chemicals were analytically pure from commercial sources and used without further purification. B_2O_3, Rb_2CO_3, and Cs_2CO_3 were purchased from the Shanghai Reagent Factory (AR); SeO_2 (AR) were purchased from Acros Organics.

Both compounds (prism in shape and colorless) were initially obtained by high temperature solid state reactions of a mixture of A_2CO_3 (A = Rb, Cs), SeO_2 and B_2O_3 which were sealed into evacuated quartz tubes without grind. The loaded compositions are as follows: Rb_2CO_3 (0.2310 g, 1 mmol), SeO_2 (0.3327 g, 3 mmol) and B_2O_3 (0.0618 g, 1mmol) for $RbSe_3B_2O_9(OH)$; Cs_2CO_3 (0.462 g, 0.5 mmol), SeO_2 (0.3327 g, 3 mmol) and B_2O_3 (0.0618 g, 1mmol) for $CsSe_3B_2O_9(OH)$. Single crystals of each compound were obtained at different reaction temperatures. The mixtures were heated at 250 °C(for $RbSe_3B_2O_9(OH)$) and 230 °C (for $CsSe_3B_2O_9(OH)$) for 5 days, then cooled to 50 °C at a cooling rate of 2 °C/hr before furnaces were switched off. The average atomic ratios of Se:Rb and Se: Cs determined by EDS on several single crystals of each compound are 3.1 and 2.9 for $RbSe_3B_2O_9(OH)$ and $CsSe_3B_2O_9(OH)$, respectively, which are in good agreement with those determined from single-crystal X-ray structure studies. The SEM images with different magnification should be provided to show the morphology of the products (Figure S1). After single crystal structural analyses, pure powder samples of $RbSe_3B_2O_9(OH)$ and $CsSe_3B_2O_9(OH)$ were obtained from the stoichiometric mixtures of A_2CO_3 (A = Rb, Cs), SeO_2, and B_2O_3 at 150 °C and 150 °C for 6 days for $RbSe_3B_2O_9(OH)$ and $CsSe_3B_2O_9(OH)$, respectively. Their purities were confirmed by XRD powder diffraction studies (Figure S2).

2. Structure determination

Data collections were performed on Xcalibur, Eos CCD (for $RbSe_3B_2O_9(OH)$) and Rigaku Saturn724+ CCD (for $CsSe_3B_2O_9(OH)$) diffractometers equipped with a graphite-monochromated Mo-Kα radiation (λ = 0.71073 Å) at 293(2) K. Both data sets were corrected for Lorentz and polarization factors as well as for absorption by Multi-scan method.[1]

Structures were solved by the direct methods and refined by full-matrix least-squares fitting on F^2 by SHELX-97.[2] All of the non-hydrogen atoms were refined with anisotropic thermal parameters except B(1), O(2), O(6) and O(10) in $RbSe_3B_2O_9(OH)$ and B(1), B(2), O(1) and O(3) in $CsSe_3B_2O_9(OH)$, which were refined isotropically due to their large ADP max/min ratios. The refinements of $RbSe_3B_2O_9(OH)$ were poor due to its poor crystal quality. However, since it is isostructural with $CsSe_3B_2O_9(OH)$, no attempts were made to improve its refinements. Both date sets of $RbSe_3B_2O_9(OH)$ and $CsSe_3B_2O_9(OH)$ were performed TWIN refinements. The Flack factors for $RbSe_3B_2O_9(OH)$ and $CsSe_3B_2O_9(OH)$ are 0.49(5) and 0.56(2), respectively, indicate the existence of the racemic twinning. These are proved by the refinements of several data sets collected on different crystals. O(5) in $RbSe_3B_2O_9(OH)$ and $CsSe_3B_2O_9(OH)$ are protonated based on the requirement of charge balance and bond-valence calculations; their calculated bond valences are 1.40 and 1.39 respectively. Both H atoms were located at geometrically calculated positions and refined with isotropic thermal parameters. The structures were also checked for possible missing symmetry with PLATON.[3] Crystallographic data and structural refinements for both compounds are summarized in Table 1. Important bond distances are listed in Table S1. More details on the crystallographic studies as well as atomic displacement parameters in this paper have been deposited in the Cambridge Crystallographic Data Center as supplementary publication, CCDC Nos. 424272 and 424273 for compounds $RbSe_3B_2O_9(OH)$ and $CsSe_3B_2O_9(OH)$, respectively.

3. Physical Properties Measurements

X-Ray powder diffraction (XRD) patterns were collected on a XPERT-MPD θ–2θ diffractometer using graphite-monochromated Cu-Kα radiation in the 2θ range of 5–65˚ with a step size of 0.02˚.

Microprobe elemental analyses were performed on a field-emission scanning electron microscope (JSM6700F) equipped with an energy-dispersive X-ray spectroscope (EDS, Oxford INCA).

Thermogravimetric analysis (TGA) and differential thermal analysis (DTA) studies were carried out with a NETZSCH STA 449 F3 unit at a heating rate of 10 °C/min under a nitrogen atmosphere.

IR spectra were recorded on a Magna 750 FT-IR spectrometer as KBr pellets in the range of 4000–400 cm^{-1}.

The UV–visible sbsorption and optical diffuse-reflectance spectra were measured at room temperature with a PE Lambda 900 UV–visible spectrophotometer. The $BaSO_4$ plate was used as a standard (100% reflectance). The absorption spectrum was calculated from reflectance spectrum using the Kubelka–Munk function: $\alpha/S = (1-R)^2/2R$,[4] where α is the absorption coefficient, S is the scattering coefficient, which is practically wavelength-independent when the particle size is larger than 5 *μ*m, and R is the reflectance.

Measurements of the powder frequency-doubling effect were carried out by means of the modified method of Kurtz and Perry.[5] A 1064 nm radiation generated by a Q-switched Nd:YAG solid-state laser was used as the fundamental frequency light. The SHG wavelength is 532 nm. The SHG efficiency has been shown to depend strongly on particle size; thus, the sample was ground and sieved into several distinct particle size ranges (53–75, 75–105, 105–150 and 150–210 μm). Sieved KDP powder (150–210 μm) was used as a reference materials to assume the SHG effect.

4. **Computational Descriptions**

Band structures and density of states (DOS) were performed with the total-energy code CASTEP.[6] The total energy is calculated with density functional theory (DFT) using Perdew-Burke-Ernzerh of generalized gradient approximation.[7] The interactions between the ionic cores and the electrons are described by the norm-conserving pseudopotential.[8] The following orbital electrons are treated as valence electrons: Rb-$4s^2 4p^6 5s^1$, Cs-$5s^2 5p^6 6s^1$, Se-$4s^2 4p^2$, B-$2s^2 2p^1$, and O-$2s^2 2p^4$. The number of plane waves included in the basis is determined by a cutoff energy of 500 eV, and the numerical integration of the Brillouin zone is performed using a Monkhorst-Pack *k*-point sampling of 5×2×2. The other calculating parameters and convergent criteria were the default values of CASTEP code.

The calculations of linear optical properties in terms of the complex dielectric function $\varepsilon(\omega) = \varepsilon_1(\omega) + i\varepsilon_2(\omega)$ were made. The imaginary part of the dielectric function ε_2 was given in the following equation.[9]

$$\varepsilon_2^{ij}(\omega) = \frac{8\pi^2\hbar^2e^2}{m^2V}\sum_k\sum_{cv}(f_c - f_v)\frac{p_{cv}^i(k)p_{vc}^j(k)}{E_{vc}^2}\delta\left[E_c(k) - E_v(k) - \hbar\omega\right] \qquad (1)$$

The second-order optical properties were calculated based on momentum-gauge formalism with the minimal-coupling interaction Hamiltonian and within the independent-particle approximation.[10] The imaginary part of the frequency-dependent second-order susceptibility $\chi^{(2)}(2\omega,\omega,\omega)$ is obtained from the electronic band structures by using the expressions already given elsewhere. Then use the Kramers-Kronig relations, as required by causality, to obtain the real part

$$\chi'^{(2)}(-2\omega,\omega,\omega) = \frac{2}{\pi}P\int_0^{\infty}d\omega'\frac{\omega'\chi''^{(2)}(2\omega',\omega',\omega')}{\omega'^2 - \omega^2} \qquad (2)$$

In the present study, the δ function in the expressions for $\chi^{(2)}(2\omega,\omega,\omega)$ is approximated by a Gaussian function with Γ= 0.2 eV. Furthermore, to ensure that the real part calculated via Kramer-Kronig transformation (Eq. 2) is reliable, at least 300 empty bands were used in SHG calculation. In addition, because DFT-GGA fails to correctly predict the CB energies, so the CB energy should be corrected by adding a scissor operator, meanwhile, the momentum matrix elements were also renormalized. [11]

5. Reference

[1] *CrystalClear*, Version 1.3.5; Rigaku Corp.: Woodlands, TX, 1999.

[2] G.M. Sheldrick, *SHELXTL*, *Crystallographic Software Package*, Version 5.1; Bruker-AXS: Madison, WI, 1998.

[3] A.L. Spek, PLATON; Utrecht University: Utrecht, Netherlands, 2001**.**

[4] W.M. Wendlandt, and H.G. Hecht, *Reflectance Spectroscopy*; Interscience: New York,

1966.

[5] S.K. Kurtz, and T.T. Perry, *J. Appl. Phys.*, 1968, **39**, 3798.

[6] a) M.D. Segall, P.J.D. Lindan, M.J. Probert, C.J. Pickard, P.J. Hasnip, S.J. Clark, and M.C. Payne, *J. Phys.: Condens. Matt.*, 2002, **14**, 2717; b) V. Milman, B. Winkler, J.A. White, C.J. Pickard, M.C. Payne, E.V. Akhmatskaya, and R.H. Nobes, *Int. J. Quantum Chem.*, 2000, **77**, 895.

[7] J.P. Perdew, K. Burke, and M. Ernzerhof, *Phys. Rev. Lett.*, 1996, **77**, 3865.

[8] J.S. Lin, A. Qteish, M.C. Payne, and V. Heine, *Phys. Rev. B,* 1993, **47**, 4174.

[9] F. Bassani, and G.P. Parravicini, *Electronic States and Optical Transitions In Solids;* Pergamon Press Ltd.: Oxford, 1975.

[10] a) E. Ghahramani, D.J. Moss, and J.E. Sipe, *Phys. Rev. B*, 1991, **43**, 8990; b) E. Ghahramani, D.J. Moss, and J.E. Sipe, *Phys. Rev. Lett.*, 1990, **64**, 2815.

[11] a) C.G. Duan, J. Li, Z.Q. Gu, and D.S. Wang, *Phys. Rev. B,* 1999, **60**, 9435; b) G.Y. Guo, K.C. Chu, D.S. Wang, and C.G. Duan, *Phys. Rev. B,* 2004**, 69**, 205416; c) G. Y. Guo, and J.C. Lin, *Phys. Rev. B,* 2005, **72**, 075416.

Table S1. Important bond lengths (Å) for the $RbSe_3B_2O_9(OH)$ and $CsSe_3B_2O_9(OH)$[a]

$RbSe_3B_2O_9(OH)$			
Se(1)-O(10)	1.62(1)	B(1)-O(3)	1.41(2)
Se(1)-O(1)	1.71(1)	B(1)-O(8)	1.46(2)
Se(1)-O(5)	1.74(1)	B(1)-O(2) #1	1.52(2)
		B(1)-O(4)	1.52(2)
Se(2)-O(8)	1.69(1)		
Se(2)-O(6)	1.70(1)	B(2)-O(3)	1.40(2)
Se(2)-O(7)	1.71(1)	B(2)-O(1)	1.48(2)

		B(2)-O(5) #1	1.49(2)
Se(3)-O(9)	1.628(9)	B(2)-O(6)	1.52(2)
Se(3)-O(4)	1.68(1)		
Se(3)-O(2)	1.75(1)		
$CsSe_3B_2O_9(OH)$			
Se(1)-O(10)	1.635(4)	B(1)-O(3)	1.403(8)
Se(1)-O(1)	1.739(4)	B(1)-O(8)	1.497(8)
Se(1)-O(5)	1.748(4)	B(1)-O(2) #1	1.505(8)
		B(1)-O(4)	1.505(8)
Se(2)-O(8)	1.702(4)		
Se(2)-O(6)	1.711(4)	B(2)-O(3)	1.436(7)
Se(2)-O(7)	1.719(4)	B(2)-O(5) #1	1.467(7)
		B(2)-O(1)	1.472(8)
Se(3)-O(9)	1.641(4)	B(2)-O(6)	1.526(7)
Se(3)-O(4)	1.721(5)		
Se(3)-O(2)	1.747(4)		

[a] Symmetry transformations used to generate equivalent atoms: #1 x-1, y, z.

Table S2. Assignments of IR absorption peaks for $RbSe_3B_2O_9(OH)$ and $CsSe_3B_2O_9(OH)$.

Mode descriptions (cm-1)	RbSe3B2O9(OH)	CsSe3B2O9(OH)
Asymmetrical stretch of BO_4 groups	1170, 1095, 975, 883	1168, 1098, 971, 883
Asymmetrical stretch of SeO_3 units	834, 762, 709	831, 758, 708
Bending vibrations of Se-O bonds	553	552
Bending vibrations of B-O bonds	550-634	550-632

Table S3. The state energies (eV) of the lowest conduction band (LCB) and the highest valence band (HVB) of $RbSe_3B_2O_9(OH)$, and $CsSe_3B_2O_9(OH)$.

Compound	k-point	L-CB	H-VB
$RbSe_3B_2O_9(OH)$	G (0.000, 0.000, 0.000)	4.09612	-0.07586
	Z (0.000, 0.000, 0.500)	4.15041	-0.08967
	T (-0.500, 0.000, 0.500)	3.75029	-0.01278
	Y (-0.500, 0.000, 0.000)	3.7416	-0.00226
	S (-0.500, 0.500, 0.000)	3.73939	0
	X (0.000, 0.500, 0.000)	4.19327	-0.14453
	U (0.000, 0.500, 0.500)	4.19232	-0.14622
	R (-0.500, 0.500, 0.500)	3.75215	-0.01837
$CsSe_3B_2O_9(OH)$	G (0.000, 0.000, 0.000)	4.21864	-0.08268
	Z (0.000, 0.000, 0.500)	4.26534	-0.08794
	T (-0.500, 0.000, 0.500)	3.84865	-0.01261
	Y (-0.500, 0.000, 0.000)	3.84352	-0.00276
	S (-0.500, 0.500, 0.000)	3.85022	0
	X (0.000, 0.500, 0.000)	4.31483	-0.11387
	U (0.000, 0.500, 0.500)	4.31311	-0.11219
	R (-0.500, 0.500, 0.500)	3.86704	-0.01826

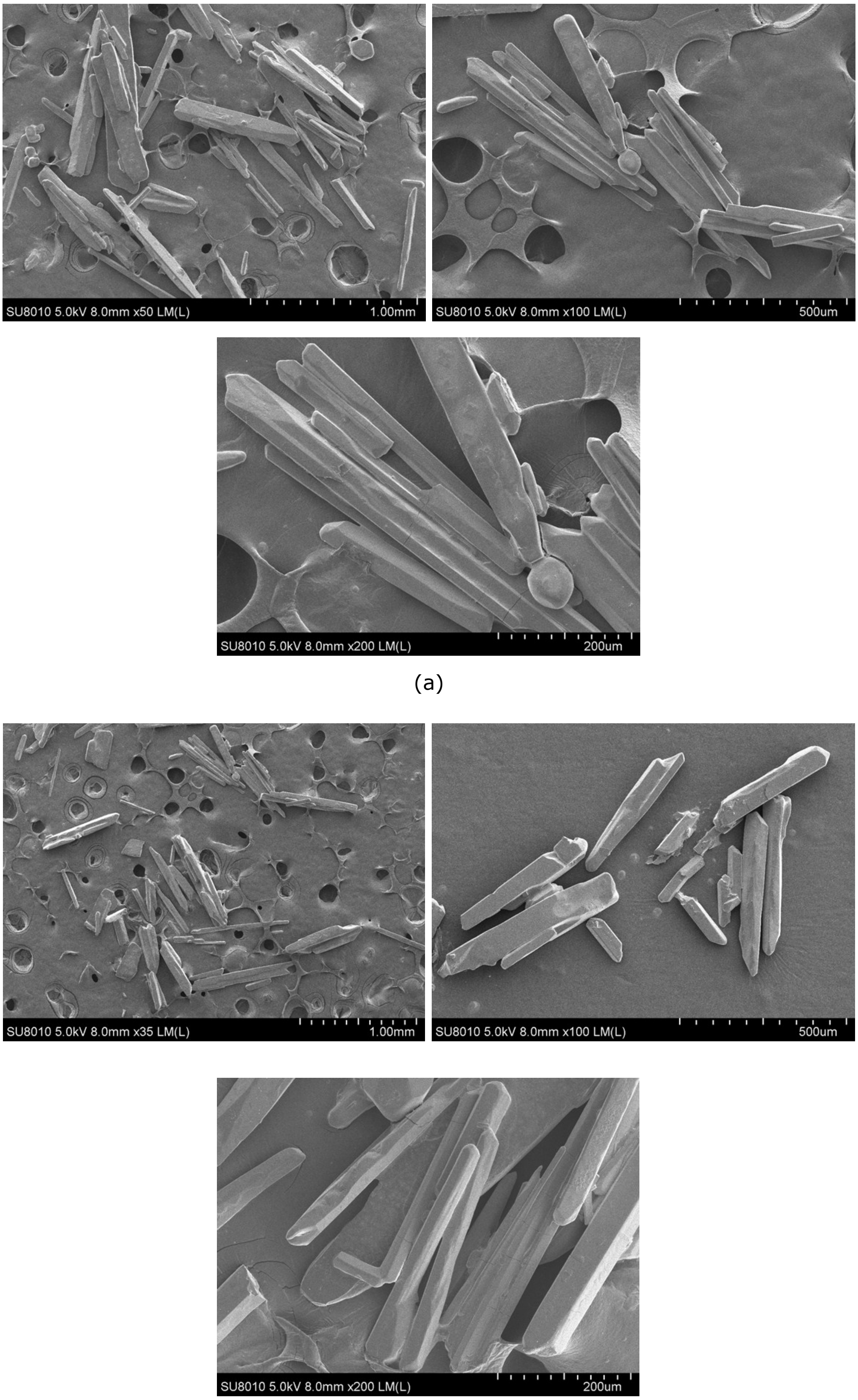

(a)

(b)

Figure S1. SEM images with different magnification for $RbSe_3B_2O_9(OH)$ (a) and $CsSe_3B_2O_9(OH)$ (b).

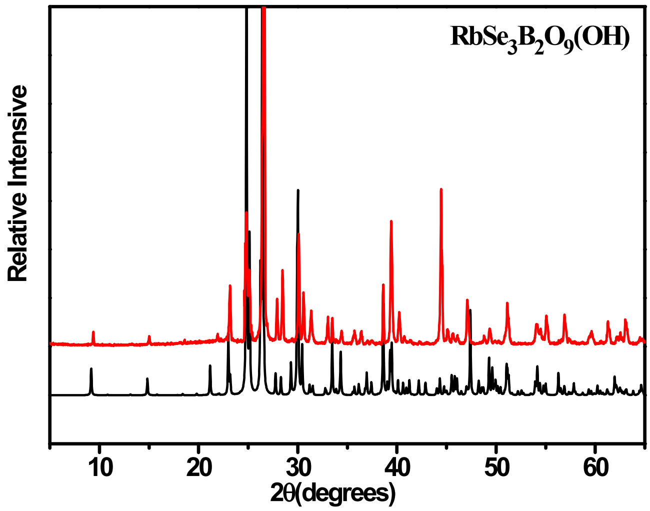

(a)

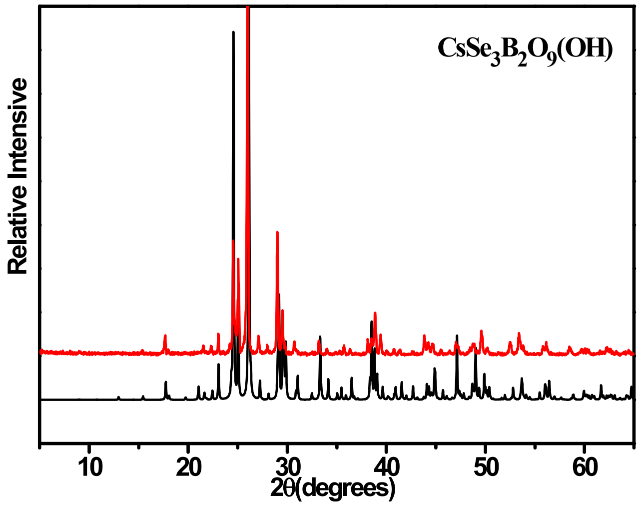

(b)

Figure S2. Simulated and measured XRD powder patterns for RbSe$_3$B$_2$O$_9$(OH) (a) and CsSe$_3$B$_2$O$_9$(OH) (b).

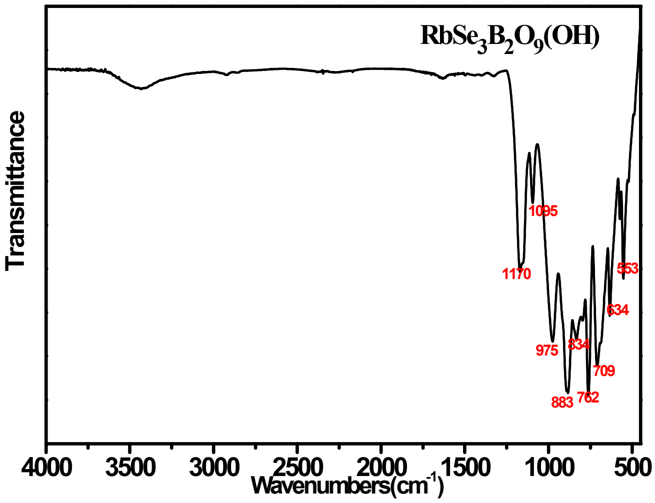

(e)

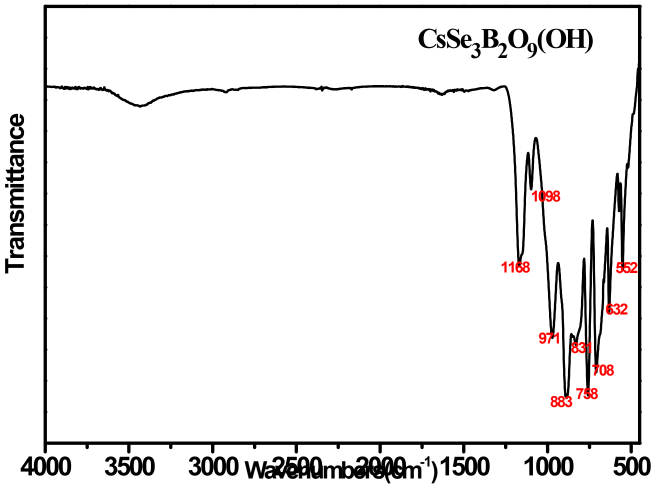

(f)

Figure S3. IR spectra for $RbSe_3B_2O_9(OH)$ (a) and $CsSe_3B_2O_9(OH)$ (b).

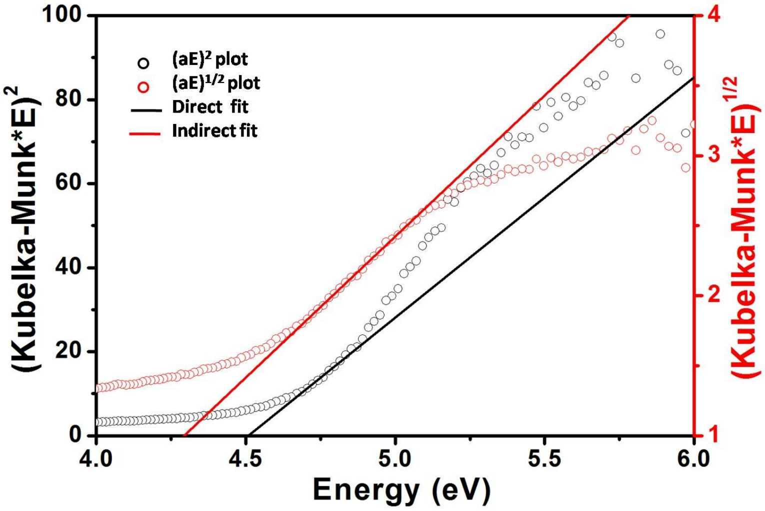

(a)

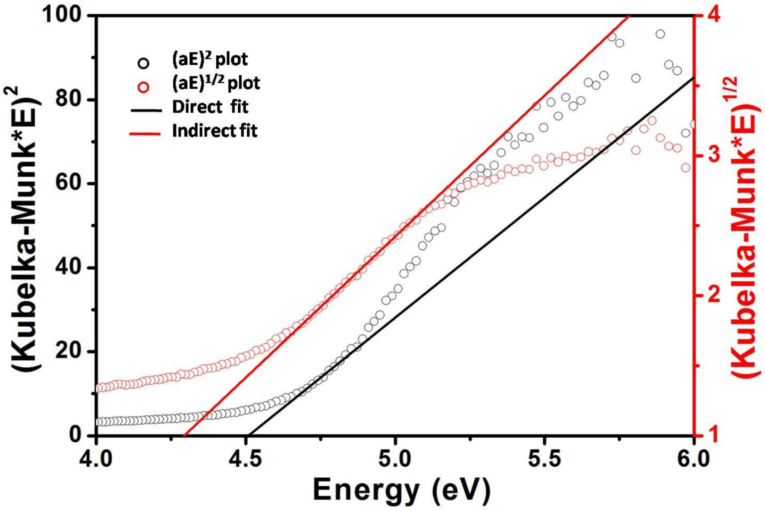

(b)

Figure S4. Diffuse reflectance UV-vis-NIR spectra for $RbSe_3B_2O_9(OH)$ (a) and $CsSe_3B_2O_9(OH)$ (b) are scaled to emphasize direct and indirect optical transitions. The degree of linear overlapping suggests the type of optical transition.

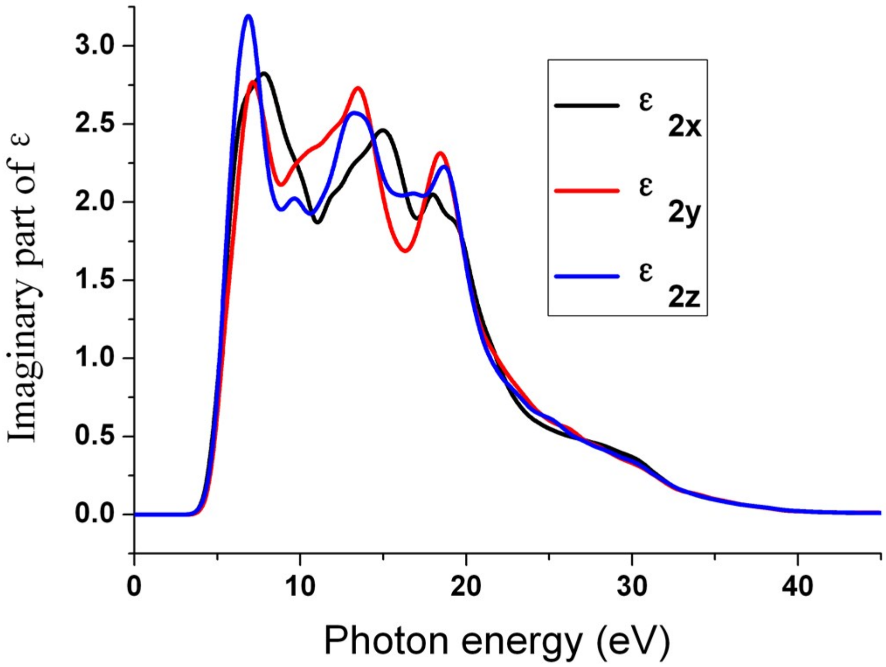

(a)

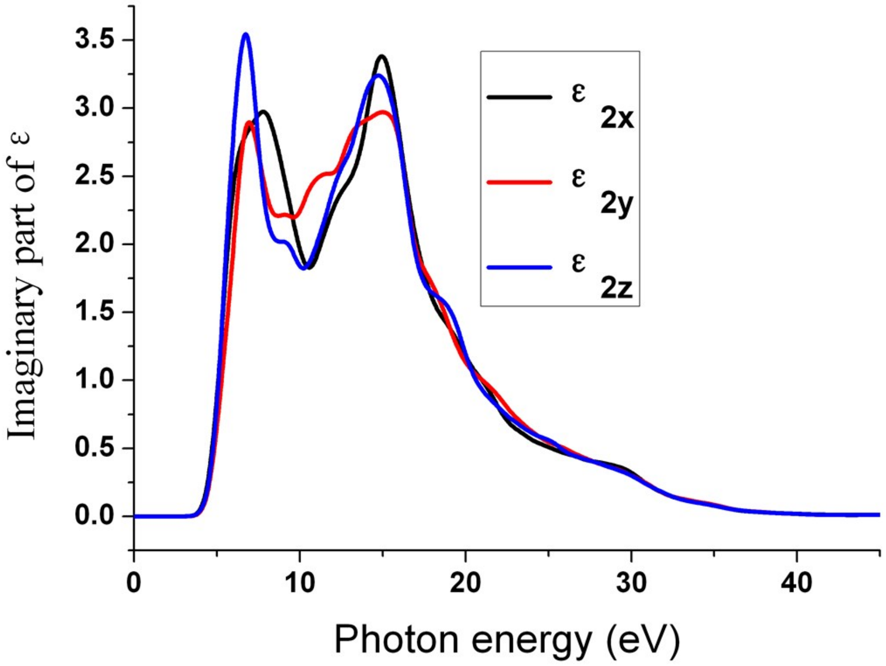

(b)

Figure S5. The imaginary parts of the frequency-dependent dielectric function of $RbSe_3B_2O_9(OH)$ (a) and $CsSe_3B_2O_9(OH)$ (b).

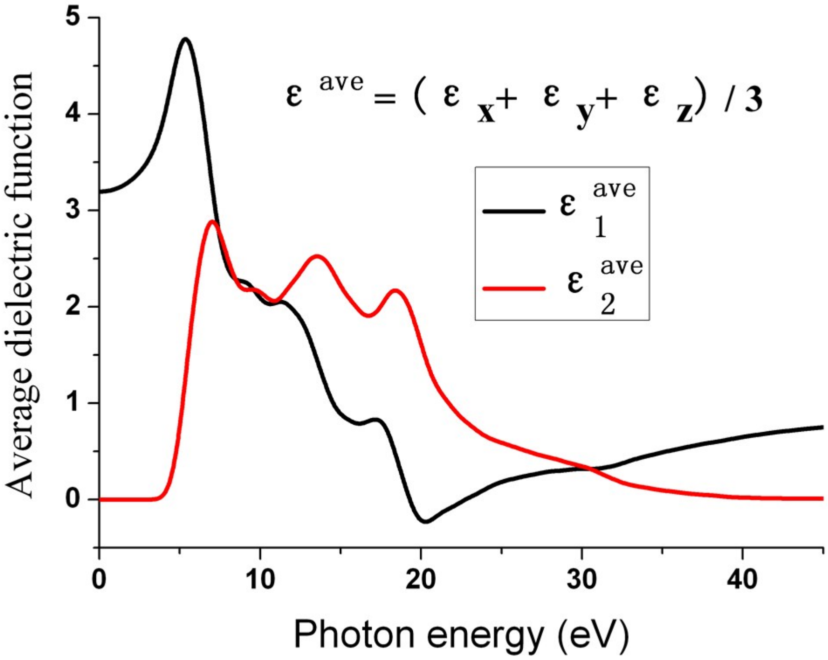

(a)

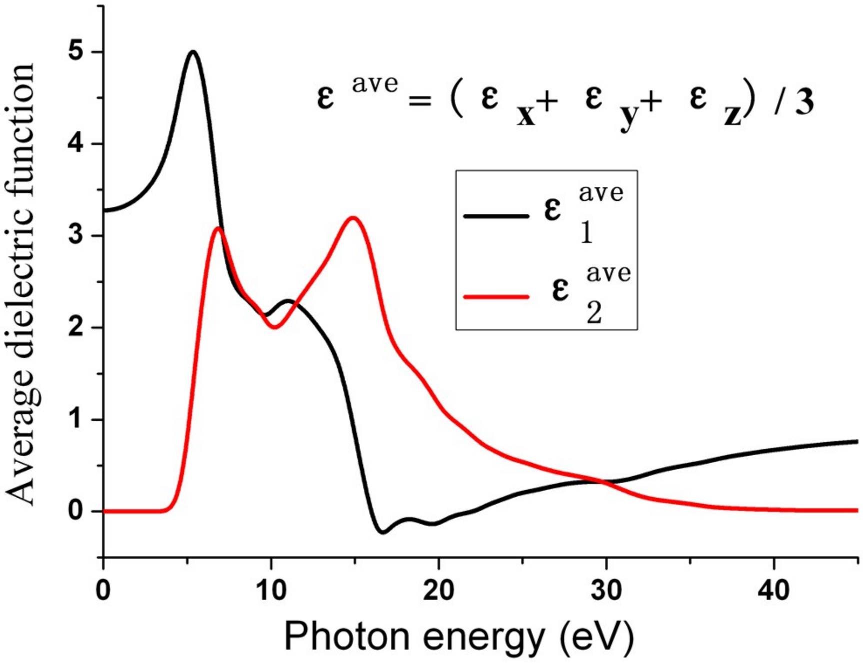

(b)

Figure S6. The curves of the averaged imaginary part and real part of dielectric function of $RbSe_3B_2O_9(OH)$ (a) and $CsSe_3B_2O_9(OH)$ (b).

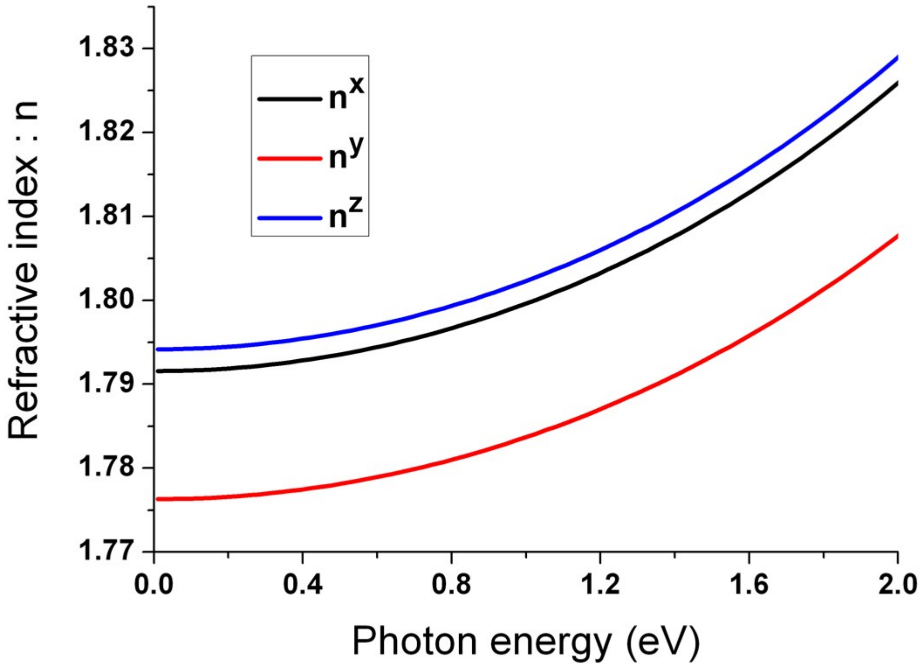

(a)

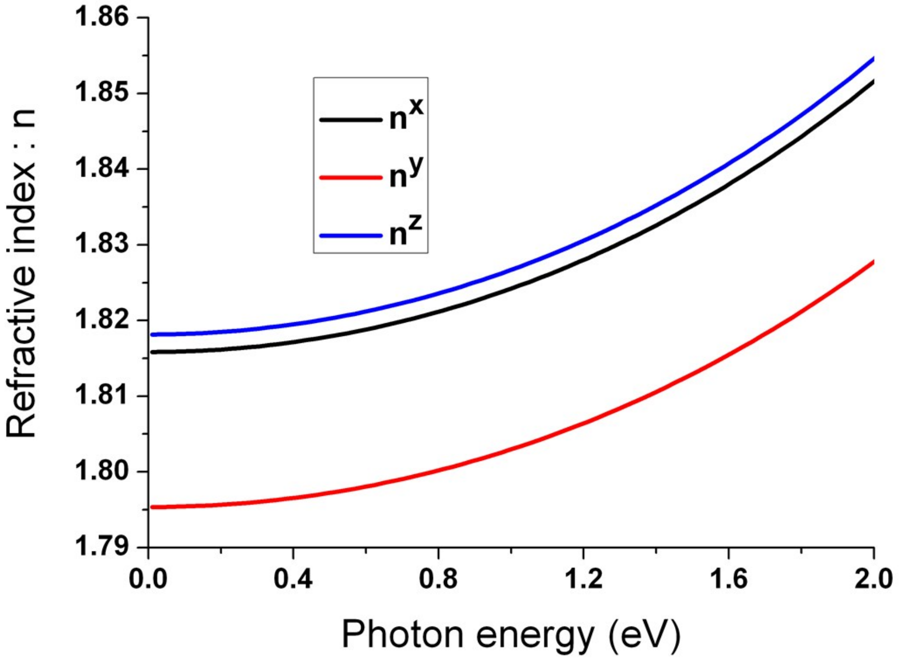

(b)

Figure S7. The dispersion of refractive index of $RbSe_3B_2O_9(OH)$ (a) and $CsSe_3B_2O_9(OH)$ (b).